Available online at www.sciencedirect.com
SCIENCE DIRECT®
Composite Structures 67 (2005) 239–249
COMPOSITE STRUCTURES
www.elsevier.com/locate/compstruct

Structural damage identification in laminated structures using FRF data

J.V. Araújo dos Santos, C.M. Mota Soares *, C.A. Mota Soares, N.M.M. Maia

IDMEC/IST, Instituto Superior Técnico, Av. Rovisco Pais, 1049-001 Lisbon, Portugal

Available online 5 November 2004

Abstract

A damage identification technique based on frequency response functions (FRF) sensitivities is presented. This technique leads to a set of linear equations, which is solved using an algorithm that constrains the solution to be physically admissible. Damage simulation and identification on a laminated rectangular plate is performed. The influence of the number of natural frequencies and mode shapes used on the FRF computation, as well as the frequency range, the excitation location and the number of measured degrees of freedom (m-DOF) is studied. Numerical tests show that the best accuracy is obtained when using the dynamic expansion of the m-DOF. It is also demonstrated that for small damage the errors are the main influence, whereas for large damage the model incompleteness becomes the most important factor in the results. A procedure for weighting and deletion of equations is used to obtain better identification results. The results of the technique presented in this paper versus those obtained by a technique based on modal data is also discussed.

Keywords: Damage identification; Frequency response functions; Model incompleteness; Measurement noise and error; Static and dynamic expansions; Laminated plate

1. Introduction

The damage identification in composites laminates is of great importance, since, for example, delaminations may not be detected by visual means and can cause catastrophic failure if not detect in due time. One knows that the occurrence of damage in structures modifies some of its mass, stiffness and damping properties, therefore changing the vibrational response of the structure. Hence, the knowledge of the vibrational behaviour of a structure can be used to determine the existence as well as the location and extent of damage.

There are two main types of damage detection techniques: (i) non-parametric and (ii) parametric. The former detect damage using direct quantities such as natural frequencies and mode shapes, frequency response functions (FRF), stiffness and flexibility matrices. The latter use a set of parameters which define the model of the structure and the assumed damage mechanisms. Several kinds of parameterizations may be employed. Among them are sub-structural, physical and geometric parameters, generic elements and stiffness parameters. A report by Doebling et al. [1] surveys both techniques, which are applied to several kind of structures. Zou et al. [2] present a review of vibration-based model dependent techniques for the identification of delaminations in composite structures. An important class of parametric methods use sensitivity analysis of modal data (natural frequencies and mode shapes) [3–12] or FRF data [13–15] to update structural models or identify damage. In these techniques, the derivatives of the data, namely natural frequencies, mode shapes and FRF, with respect to the physical parameters, lead

* Corresponding author. Tel.: +351 21 841 7455; fax: +351 21 841 7915.
E-mail address: cmmsoares@alfa.ist.utl.pt (C.M. Mota Soares).

0263-8223/$ - see front matter © 2004 Elsevier Ltd. All rights reserved.
doi:10.1016/j.compstruct.2004.09.011

to the determination of a damage parameter vector. The use of the frequency response model for damage identification leads to more equations than the use of the modal model. Hence, as the number of updating parameters or damage elements unknowns increases the FRF sensitivity techniques present better results. Furthermore, the techniques based on modal data need modal extraction, which leads to errors and omissions, and the increased modal density at high frequencies can pose a problem.

The formulation of a parametric technique that uses FRF data, leading to a set of linear equations, was first presented and applied to model updating by Lin and Ewins [13]. These authors used replacement of unmeasured degrees of freedom (u-DOF) of the experimental FRF by their analytical counterparts and an iterative process to solve the set of equations. Wang et al. [14] used this technique to (i) update the undamaged structural model and (ii) identify damage in a plane 3-bay frame structure. The results presented show false negative elements (elements with an increase in stiffness), since the unknown variables are not constrained. In case of damage, there would be elements with only a decrease in stiffness. In the present work, the set of equations is solved by constraining the variables to be physically admissible, i.e., the solution is such that there are no false negative elements.

A problem often encountered in this methods is the model incompleteness of the damaged structure, because the vibrational characteristics should be obtained experimentally and, for example, the rotational degrees of freedom are very difficult to measure. As a result, the total number of undamaged structure degrees of freedom (t-DOF), computed analytically, exceeds the number of damaged structure measured degrees of freedom (m-DOF). Furthermore, due to measurement noises and other uncertainties, the FRF m-DOF are always contaminated to some extent with errors. In this work, the problem of model incompleteness is dealt with two methods: (i) dynamic and (ii) static expansions of m-DOF. These methods are based on the dynamic [16] and static [17] reduction methods, respectively. By imposing a random perturbation in the amplitudes of the m-DOF of the damaged structure, the presence of errors was also taken into account.

A laminated rectangular plate free in space, which is discretised using a first-order shear-deformation theory (FSDT) based element [18], was used to perform the numerical tests. It is shown that the number of natural frequencies and mode shapes used on the FRF computation, the frequency range and the excitation location are important factors in the accuracy of the identification results. The results of the technique presented in this paper are compared to those obtained by a technique based on modal data [12].

2. Damage identification technique

2.1. FRF computation

The FRF matrix $\mathbf{A}(\omega)$ of the undamaged structure can be defined in terms of the modal model, i.e., in terms of a specified number of its natural frequencies and mode shapes, as

$$\mathbf{A}(\omega) = \mathbf{Q}(\boldsymbol{\Delta\omega})^{-1}\mathbf{Q}^{\mathrm{T}}, \tag{1}$$

where

$$\mathbf{Q} = \begin{bmatrix} q_{11} & q_{12} & \cdots & q_{1(n-1)} & q_{1n} \\ q_{21} & q_{22} & \cdots & q_{2(n-1)} & q_{2n} \\ \vdots & \vdots & \vdots & \vdots & \vdots \\ q_{(Ng-1)1} & q_{(Ng-1)2} & \cdots & q_{(Ng-1)(n-1)} & q_{(Ng-1)n} \\ q_{Ng1} & q_{Ng2} & \cdots & q_{Ng(n-1)} & q_{Ngn} \end{bmatrix} \tag{2}$$

is the modal matrix, where the first and second subscripts denote, respectively, the DOF and the mode shape.

$\boldsymbol{\Delta\omega}$ is a diagonal matrix, defined as

$$\boldsymbol{\Delta\omega} = \begin{bmatrix} \lambda_1 - \omega^2 & 0 & \ldots & 0 & 0 \\ 0 & \lambda_2 - \omega^2 & \ldots & 0 & 0 \\ \vdots & \vdots & \vdots & \vdots & \vdots \\ 0 & 0 & \ldots & \lambda_{n-1} - \omega^2 & 0 \\ 0 & 0 & \ldots & 0 & \lambda_n - \omega^2 \end{bmatrix}, \tag{3}$$

where the subscript in λ denotes the squared natural frequency and ω is the excitation frequency.

Matrices $\mathbf{Q}$ and $\boldsymbol{\Delta\omega}$ have dimensions $Ng \times n$ and $n \times n$, respectively, where Ng is the total degrees of freedom (t-DOF) and n is the number of computed natural frequencies and mode shapes of the undamaged structure. Therefore, the FRF matrix $\mathbf{A}(\omega)$ has order Ng, but a rank of n. Note that the structure has no damping. Matrix $\mathbf{Q}$ and the eigenvalues λ_i are computed using finite element analysis.

Similarly, one can compute the FRF matrix $\widetilde{\mathbf{A}}(\omega)$ of the damaged structure as follows:

$$\widetilde{\mathbf{A}}(\omega) = \widetilde{\mathbf{Q}}(\boldsymbol{\Delta\tilde{\omega}})^{-1}\widetilde{\mathbf{Q}}^{\mathrm{T}}, \tag{4}$$

where

$$\widetilde{\mathbf{Q}} = \begin{bmatrix} \tilde{q}_{11} & \tilde{q}_{12} & \cdots & \tilde{q}_{1(m-1)} & \tilde{q}_{1m} \\ \tilde{q}_{21} & \tilde{q}_{22} & \cdots & \tilde{q}_{2(m-1)} & \tilde{q}_{2m} \\ \vdots & \vdots & \vdots & \vdots & \vdots \\ \tilde{q}_{(Ng-1)1} & \tilde{q}_{(Ng-1)2} & \cdots & q_{(Ng-1)(m-1)} & \tilde{q}_{(Ng-1)m} \\ \tilde{q}_{Ng1} & \tilde{q}_{Ng2} & \cdots & \tilde{q}_{Ng(m-1)} & \tilde{q}_{Ngm} \end{bmatrix} \tag{5}$$

and

$$\mathbf{\Delta\tilde{\omega}} = \begin{bmatrix} \tilde{\lambda}_1 - \omega^2 & 0 & \dots & 0 & 0 \\ 0 & \tilde{\lambda}_2 - \omega^2 & \dots & 0 & 0 \\ \vdots & \vdots & \vdots & \vdots & \vdots \\ 0 & 0 & \dots & \tilde{\lambda}_{m-1} - \omega^2 & 0 \\ 0 & 0 & \dots & 0 & \tilde{\lambda}_m - \omega^2 \end{bmatrix}. \tag{6}$$

Now, matrices $\widetilde{\mathbf{Q}}$ and $\mathbf{\Delta\tilde{\omega}}$ have dimensions $Ng \times m$ and $m \times m$, respectively, where m is the number of computed natural frequencies and mode shapes of the damaged structure. In this case, the FRF matrix $\widetilde{\mathbf{A}}(\omega)$ rank m.

2.2. FRF sensitivities

Considering that a single-input unit force $\mathbf{f}_l$ is applied to the lth DOF of both the undamaged and damaged structure one gets

$$\widetilde{\mathbf{Z}}(\omega)\tilde{\mathbf{a}}_l(\omega) = \mathbf{f}_l = \mathbf{Z}(\omega)\mathbf{a}_l(\omega), \tag{7}$$

where $\widetilde{\mathbf{Z}}(\omega)$ and $\mathbf{Z}(\omega)$ are the dynamic stiffness matrices of the damaged and undamaged structure, respectively. The vectors $\tilde{\mathbf{a}}_l(\omega)$ and $\mathbf{a}_l(\omega)$ are the lth column of $\widetilde{\mathbf{A}}(\omega)$ and $\mathbf{A}(\omega)$, respectively.

The above equation can be written as

$$\mathbf{\Delta Z}(\omega)\tilde{\mathbf{a}}_l(\omega) = \mathbf{f}_l - \mathbf{Z}(\omega)\tilde{\mathbf{a}}_l(\omega), \tag{8}$$

with $\mathbf{\Delta Z}(\omega) = \widetilde{\mathbf{Z}}(\omega) - \mathbf{Z}(\omega)$. The right-hand side of this expression is ill-conditioned [19] and, therefore, one must pre-multiply both sides of Eq. (8) by $\mathbf{A}(\omega)$:

$$\mathbf{A}(\omega)\mathbf{\Delta Z}(\omega)\tilde{\mathbf{a}}_l(\omega) = \mathbf{a}_l(\omega) - \tilde{\mathbf{a}}_l(\omega). \tag{9}$$

Note that $\mathbf{f}_l$ is the lth column of the identity matrix. The right-hand side of Eq. (9) is the difference between the undamaged and damaged structure FRF.

Considering a first-order Taylor expansion, the damaged dynamic stiffness $\widetilde{\mathbf{Z}}$ is given by

$$\widetilde{\mathbf{Z}}(\omega) = \mathbf{Z}(\omega) + \mathbf{\Delta Z}(\omega) = \mathbf{Z}(\omega) + \sum_{e=1}^{N} \frac{\partial \widetilde{\mathbf{Z}}(\omega)}{\partial(\delta b_e)} \delta b_e, \tag{10}$$

where N is the number of finite elements and $\delta b_e \in [0, 1[$ is the element e damage parameter.

For each finite element e

$$\frac{\partial \widetilde{\mathbf{Z}}(\omega)}{\partial(\delta b_e)} = \frac{\partial(\widetilde{\mathbf{K}} - \omega^2\mathbf{M})}{\partial(\delta b_e)} = \frac{\partial \widetilde{\mathbf{K}}}{\partial(\delta b_e)} \quad \text{for } e = 1, \dots, N, \tag{11}$$

since the mass is constant.

Defining the damaged global stiffness matrix by

$$\widetilde{\mathbf{K}} = \mathbf{K} - \delta\mathbf{K} \tag{12}$$

or, at the finite element level

$$\widetilde{\mathbf{K}}_e = \mathbf{K}_e - \delta\mathbf{K}_e = \mathbf{K}_e - \delta b_e \mathbf{K}_e, \tag{13}$$

Eq. (11) becomes

$$\frac{\partial \widetilde{\mathbf{Z}}(\omega)}{\partial(\delta b_e)} = \frac{\partial \widetilde{\mathbf{K}}}{\partial(\delta b_e)} = -\mathbf{K}_e. \tag{14}$$

Replacing (14) in (10) one gets

$$\mathbf{\Delta Z}(\omega) = \widetilde{\mathbf{Z}}(\omega) - \mathbf{Z}(\omega) = -\sum_{e=1}^{N} \mathbf{K}_e \delta b_e \tag{15}$$

and Eq. (9) can be written as

$$\sum_{e=1}^{N} \mathbf{A}_e(\omega)\mathbf{K}_e\tilde{\mathbf{a}}_{le}(\omega)\delta b_e = \tilde{\mathbf{a}}_l(\omega) - \mathbf{a}_l(\omega). \tag{16}$$

The matrix $\mathbf{A}_e(\omega)$ and the vector $\tilde{\mathbf{a}}_{le}(\omega)$ contain the entries of $\mathbf{A}(\omega)$ and $\tilde{\mathbf{a}}_l(\omega)$ relative to element e, respectively.

Expression (16) defines a set of Ng linear equations, with N unknowns. If one considers Nf excitation frequencies the number of equations increases to $M = Ng \times Nf$. In compact form, expression (16) is written as

$$\mathbf{S}\delta b = \delta\mathbf{a}. \tag{17}$$

One can use Ne single-input unit forces applied to different DOF, leading to $M = Ng \times Nf \times Ne$ equations. However, in the present work, only one single-input unit force $\mathbf{f}_l$ was applied to the lth DOF of both the undamaged and damaged structure.

The least-squares solution of (17) is given by,

$$\delta b = (\mathbf{S}^{\mathrm{T}}\mathbf{S})^{-1}\mathbf{S}^{\mathrm{T}}\delta\mathbf{a} = \mathbf{S}^{+}\delta\mathbf{a}, \tag{18}$$

where $\mathbf{S}^{+}$ is the pseudo-inverse of $\mathbf{S}$.

In the above formulation it is implicit that one knows all the DOF of the damaged structure. However, that is not possible to accomplish in practice, as, for instance, rotational DOF are very difficult to obtain experimentally. Consequently, the unknown degrees of freedom (u-DOF) of the damaged structure should be determined using an expansion of the measured degrees of freedom (m-DOF). To achieve this purpose, the m-DOF dynamic or static expansions may be used. The dynamic and static expansion processes are performed as described in [12].

2.3. Equations weighting, deletion and solving

The solution given by expression (18) depends not only on the quality of measured FRF data but also on the weighting technique applied to the equations. This weighting is needed because without it the least-squares solution is dominated by the equations with the largest coefficients. This means that the solution is dominated by the equations defined at frequencies and locations where the vibration response magnitudes are significant,

overshadowing the information at other frequencies and locations. Therefore, one should consider all the frequencies and locations. In this work, one multiplies both sides of each equation by a scaling factor so that the sum of coefficient squares in a resultant equation is unity [20].

The vector $\delta\mathbf{a}$ represents a subtraction between two quantities (e.g. $\tilde{a}_{il}(\omega_k) - a_{il}(\omega_k)$). If the ith equation, relative to the kth frequency, has elements $\tilde{a}_{il}(\omega_k)$ and $a_{il}(\omega_k)$ of similar magnitudes, the measurement error may be significantly magnified after weighting. To overcome this problem, such an equation should be removed. One deletes the ith equation if [20]

$$2\frac{|\widetilde{a}_{il}(\omega_k) - a_{il}(\omega_k)|}{|\widetilde{a}_{il}(\omega_k)| + |a_{il}(\omega_k)|} \leqslant \Delta \quad \text{for } k = 1, \ldots, Nf, \tag{19}$$

where $\Delta \in [0, 2]$. When $\Delta = 0$, no equation is deleted. When $\Delta = 2$, all the equations are deleted. The value of the equations deletion parameter Δ should be chosen in function of both error levels in the measured data and amount of measured data. If the error levels are high and the measured data are sufficient, a large Δ value may be appropriate; if the errors levels are low and the measured data are limited, a small Δ value should be chosen [20].

Besides the problem of finding reliable equations, the physical admissible solution of Eq. (17) is not always obtained using algorithms such as the singular value decompositon (SVD) [21,19], as can be seen in [6,7]. In Ref. [8] two alternative algorithms were proposed: the non-negative least-squares (NNLS) [21] and the bounded-variable least-squares (BVLS) [22]. The authors have been using this last algorithm with success in the damage identification using the sensitivities of modal characteristics with model incompleteness and errors [12].

The BVLS algorithm leads to a solution defined by

$$\min \|\mathbf{S}\delta\mathbf{b} = \delta\mathbf{a}\|_2 \quad \text{subject to } 0 \leqslant \delta\mathbf{b} \leqslant 1. \tag{20}$$

In other words, the solution is such that all the finite elements are either undamaged ($\delta b_e = 0$) or with a positive quantity of damage ($\delta b_e \leqslant 1$). The solution vector δb obtained using the SVD algorithm may contain elements with negative damage, i.e., elements with an increase of stiffness.

2.4. Damage identification accuracy indicators

In order to classify the accuracy of the results, some indicators were used. The damage missing error is defined as [23,24],

$$\text{DME} = \frac{1}{\text{NT}}\sum_{t=1}^{\text{NT}} \varepsilon_t^{\text{I}} \quad \text{for } 0 \leqslant \text{DME} \leqslant 1, \tag{21}$$

where NT is the number of true damaged elements and $\varepsilon_t^{\text{I}} = 0$ if the truly damaged element t is identified or $\varepsilon_t^{\text{I}} = 1$ otherwise. If DME = 0, then all true damaged elements are detected.

As a second accuracy indicator we chose the false alarm error [23,24],

$$\text{FAE} = \frac{1}{\text{NF}}\sum_{p=1}^{\text{NF}} \varepsilon_p^{\text{II}} \quad \text{for } 0 \leqslant \text{FAE} \leqslant 1, \tag{22}$$

where NF is the number of predicted damaged elements and $\varepsilon_p^{\text{II}} = 0$ if the predicted damaged element p is truly damaged or $\varepsilon_p^{\text{II}} = 1$ otherwise. If FAE = 0, then all predicted damaged elements are truly damaged elements.

The mean sizing error [24] defines an average value of the absolute discrepancies between the true damage parameters δb_e^{t} and the computed damage parameters δb_e^{c}:

$$\text{MSE} = \frac{1}{N}\sum_{e=1}^{N} |\delta b_e^{\text{t}} - \delta b_e^{\text{c}}| \quad \text{for } 0 \leqslant \text{MSE} < \infty. \tag{23}$$

The relative error,

$$\text{RE} = \frac{\sum_{e=1}^{N}|\delta b_e^{\text{t}}| - \sum_{e=1}^{N}|\delta b_e^{\text{c}}|}{\sum_{e=1}^{N}|\delta b_e^{\text{t}}|} \quad \text{for } 0 \leqslant \text{RE} \leqslant 1, \tag{24}$$

gives an indication of the relative discrepancies between the true and computed damage parameters.

An element is taken as damaged if $\delta b_e^{\text{c}} > 2 \times \text{MSE}$ [24]. The smallest the values of DME, FAE, MSE and RE the better the results. The first two indicators classify the results in terms of damage location, while the last two are related to the damage quantification accuracy.

3. Applications

The structure analysed is a carbon fibre reinforced epoxy rectangular plate, free in space, with a $[0]_8$ stacking sequence. The material properties of the layers, which have equal thicknesses, are presented in Table 1. The plate in-plane dimensions are shown in Fig. 1 and its thickness is 3.385 mm. In order to compute the natural frequencies and mode shapes, the plate is discretised in 12×12 finite elements based on the FSDT [18]. Therefore, one has 144 unknowns. Each element has eight nodes, with three DOF *per* node: one transverse displacement and two rotations, yielding a total of 481 nodes and 1443 DOF. A shift must be carried out, in order to make the stiffness matrix positive definite, since

Table 1
Mechanical properties of the layers

E_1 [GPa]	E_2 [GPa]	G_{12}[GPa]	G_{23} [GPa]	ν_{12}	ρ [kg/m^3]
107.4	8.3	4.2	8.8	0.384	1533.8

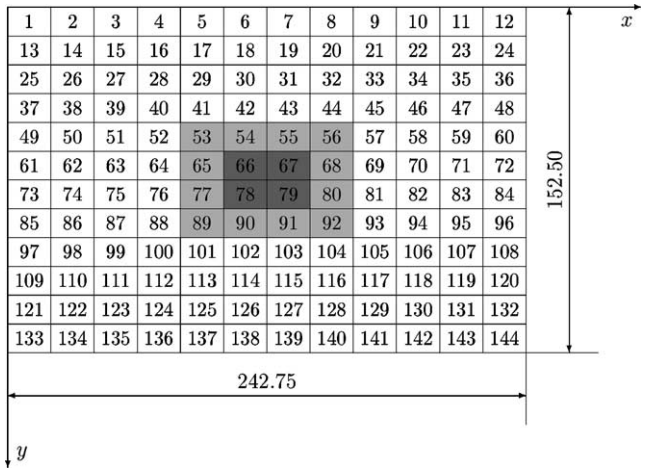

Fig. 1. Element numbering and damaged area.

the plate is free in space [25]. After the computation of natural frequencies and mode shapes, using a skyline type assemblage of matrices and the subspace iteration method [26], one uses expressions (1) and (4) to compute the FRF of the undamaged and damaged structure, respectively.

The damage was simulated in 16 elements (Fig. 1). The elements damage parameters of each of the five simulated cases are shown in Table 2, where is also presented the sum of the damage parameters, defined as

Table 2
Simulated damage cases

Element	Case 1	Case 2	Case 3	Case 4	Case 5
53, 54, 55, 56 65, 68, 77, 80 89, 90, 91, 92	0.0625	0.1250	0.2500	0.3750	0.4500
66, 67, 78, 79	0.1250	0.2500	0.5000	0.7500	0.9000
$\|\delta\mathbf{b}^r\|_1$	1.2500	2.5000	5.0000	7.5000	9.0000

$$\|\delta\mathbf{b}^t\|_1 = \sum_{e=1}^{N} |\delta b_e^t|. \tag{25}$$

Four incomplete models were considered: 481, 325, 156 and 49 transverse displacements m-DOF. The black dots in Fig. 2 indicate the nodes where these displacements are measured.

The results presented in this paper are relative to three frequency ranges: (i) [50, 1000] Hz; (ii) [1100, 1900] Hz and (iii) [50, 1900] Hz. Excitation frequencies in a range ±20 Hz from natural frequencies are eliminated. This is done because it is likely that relatively high levels of noise on the excitation signal at resonance be attained [27]. The excitation frequencies are specified such that there is a spacing of 50 Hz between two consecutive excitation frequencies. This leads to a total of 14 excitation frequencies for the first two frequency ranges and 28 for the third frequency range.

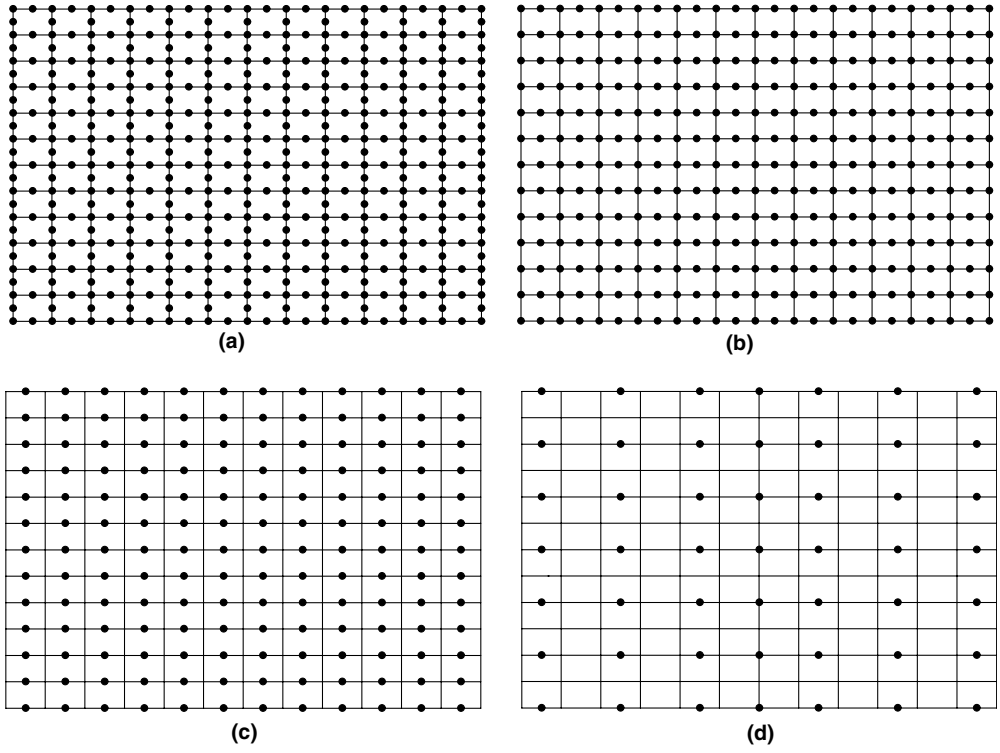

Fig. 2. Nodes with m-DOF: (a) 481 m-DOF, (b) 325 m-DOF, (c) 156 m-DOF and (d) 49 m-DOF.

3.1. Complete models

3.1.1. Without equations weighting or deletion

The following results were obtained with the knowledge of all the DOF of both undamaged and damaged structure, i.e., one knows all the *Ng* DOF.

The FRF matrices accuracy greatly depend on the number of natural frequencies and mode shapes used in their computation (see Section 2.1). Indeed, the damage identification results improve as the used number of natural frequencies and mode shapes increases (Table 3). Grafe [28] showed that the response can sufficiently be approximated by using a truncated number of frequencies and mode shapes and proposed to use a truncated modal solution of $2 \times Nm$ natural frequencies and mode shapes to approximate the response matrix in the frequency range that contains the first Nm modes. Attending to this, in the present case one can compute the matrix $\mathbf{A}(\omega)$ and the vector $\tilde{\mathbf{a}}_l(\omega)$ with sufficient accuracy using $m = n = 26$, since there are 13 natural frequencies and mode shapes in the frequency range [50, 1900] Hz. However, in view of the results in Table 3, it is better to consider more than $3 \times Nm$ natural frequencies and mode shapes.

Fig. 3 shows the differences between receptances of the undamaged structure computed with $n = 10$ and $n = 40$. One sees that there is a relative superposition of the curves for the range [0, 200] Hz and the anti-resonances decrease as the n increases. The values of the resonances are much less affected by n. This behaviour is in agreement with that found in the work of Grafe [28]. All the following damage identification results are relative to a computation of FRF with a truncated modal solution of $n = m = 40$ frequencies and mode shapes.

In Fig. 4 are presented the graphics relating the degree of damage with the absolute value of RE for the

Table 3
Accuracy indicators in function of natural frequencies and mode shapes number (3rd damage case, [50, 1900] Hz, $M = 40404$, 1441th excitation DOF)

No of frequencies and modes, m, n	DME	FAE	MSE	RE
10	0.5625	0.2222	0.0451	−0.0965
20	0.0625	0.0625	0.0145	−0.0219
30	0.1250	0.0000	0.0175	−0.0088
40	0.0000	0.0000	0.0072	−0.0012

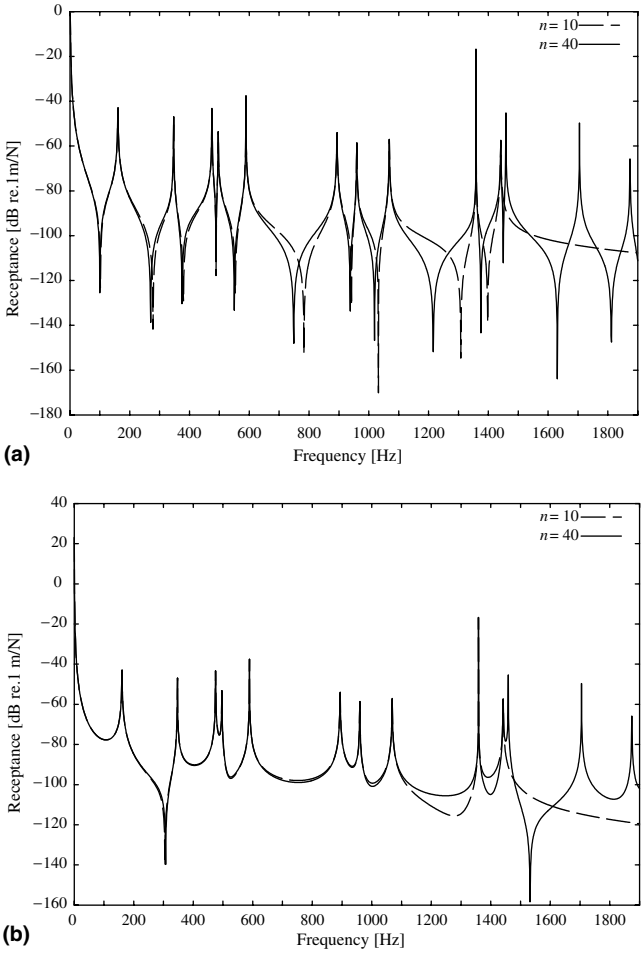

Fig. 3. Receptance curves: (a) Direct receptance (1441st DOF, 1441st DOF), (b) Transfer receptance (1441st DOF, 1st DOF).

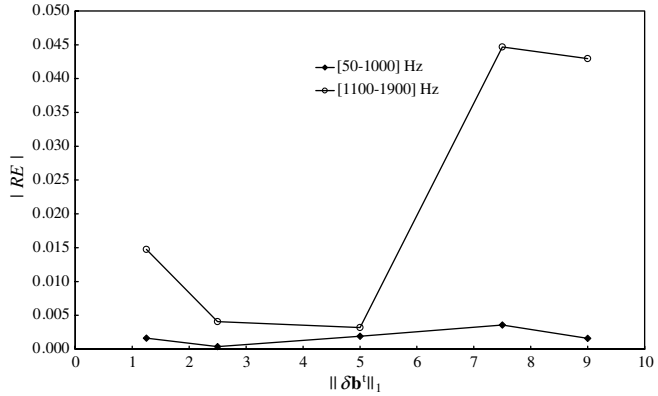

Fig. 4. Degree of damage and absolute value of RE for different frequency ranges.

frequency ranges [50, 1000] Hz and [1100–1900] Hz. Note that in both cases there are $M = 20202$ equations. One can see that the best results are obtained with the lower frequency range. This corroborates the fact that the receptances in the higher frequency range are computed with less accuracy than those in the lower frequency range. Fig. 5 shows the results for the fourth damage case with both frequency ranges. The result with the lower frequency range is indeed better than the one with the higher frequency range (Table 4). Indeed, in Fig. 5(b) there are more false identified elements (darker columns) than in Fig. 5(a).

The excitation location was also studied. Table 5 presents the accuracy indicators relative to the application of the excitation in the center (721th DOF) and the inferior right corner (1441th DOF) of the plate, for the third damage case, using the frequency range [0, 1900] Hz. In Fig. 6 one sees that the best results are in fact obtained by applying the excitation at the corner of the plate. Indeed, many modes have nodes, where the response amplitude is zero, in the center of the plate and the system of equations is more ill-conditioned when one

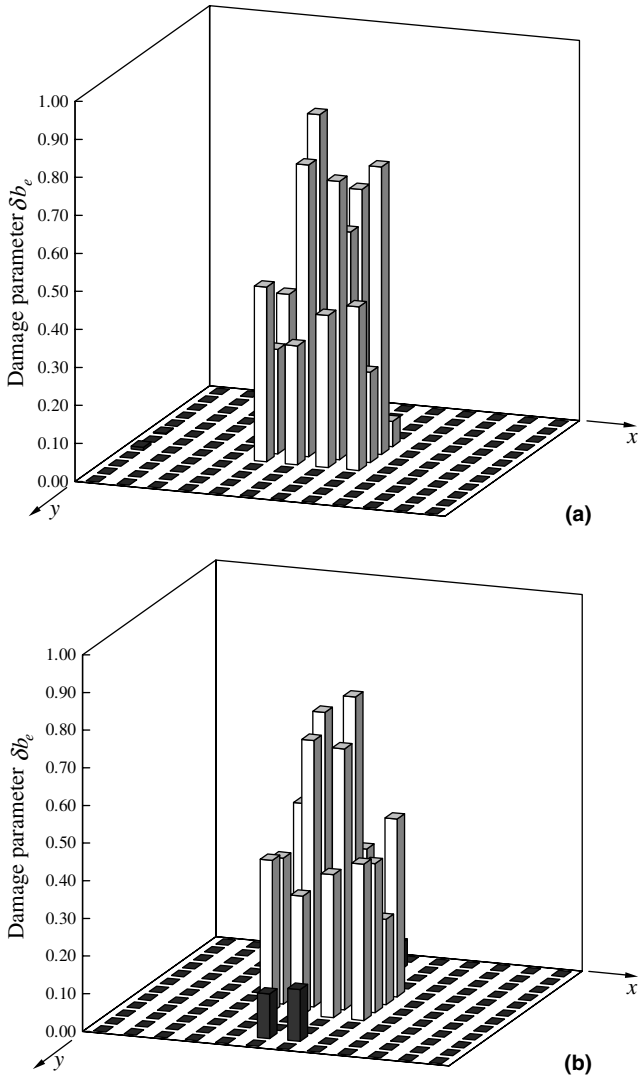

Fig. 5. Fourth damage case results with different frequency ranges ($M = 20202$): (a) [50, 1000] Hz, (b) [1100, 1900] Hz.

Table 4
Accuracy indicators in function of frequency range (4th damage case, $M = 20202$, 1441th excitation DOF)

Frequency range	DME	FAE	MSE	RE
[50, 1000] Hz	0.0000	0.0000	0.0140	−0.0036
[1100, 1900] Hz	0.0000	0.2381	0.0094	−0.0447

Table 5
Accuracy indicators in function of the excitation location (3rd damage case, $n = m = 40$, [50, 1900] Hz, $M = 40404$)

Excitation DOF	DME	FAE	MSE	RE
1441	0.0000	0.0000	0.0072	−0.0012
721	0.0000	0.1111	0.0120	−0.0087

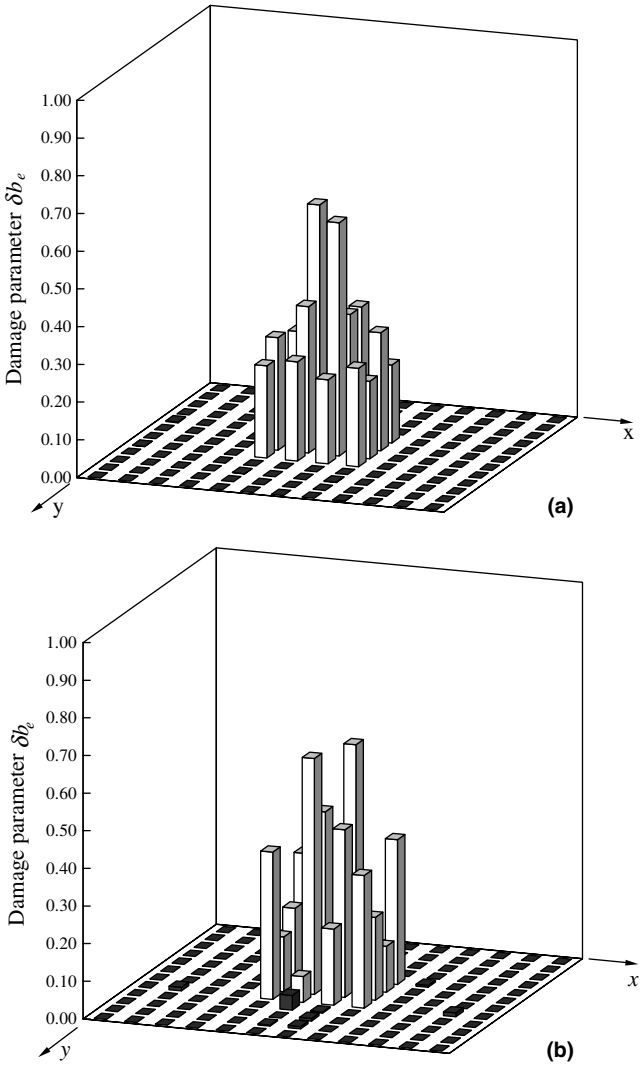

Fig. 6. Third damage case results with different excitation locations: (a) Plate inferior right corner (1441st DOF), (b) Plate center (721st DOF).

applies the excitation at this point. Hence, one must not assume a priori that the best results are obtained by applying the excitation in the damaged area.

In all the remaining Sections of this paper, the results presented were obtained using the frequency range [0, 1900] Hz, which leads to $M = 40404$ equations.

3.2. Incomplete models

3.2.1. Without errors, equations weighting or deletion

To study the differences among the dynamic and static expansions, as well as the influence of the number of m-DOF in the results, tests were performed with the four incomplete models. After the multiplications in Eq. (16), the equations relative to the u-DOF are discarded, i.e., they are not included in the damage identification process. For example, the incomplete model with 49 m-DOF leads to $M = 49 \times 28 = 1372$ equations.

Table 6 shows the DME, FAE, MSE and RE values for the third damage case. It can be seen that the best results are obtained with the dynamic expansion. As expected, when the number of m-DOF increases the accuracy indicators values decrease and the differences among the methods also become smaller. For the case of 481 m-DOF the differences between the results are not noticeable.

In Fig. 7 one can see that as the damage increases, i.e., as the sum of the true damage parameters $\|\delta\mathbf{b}^t\|_1$ increases, the error in the identification process, defined by the absolute value of RE, also increases. In fact, the difference between the stiffness matrices used in the expansion process and the real damaged structure stiffness matrices increases as the damage increases. Hence, for large damage, the vector $\tilde{\mathbf{a}}_l(\omega)$ obtained with the expansion will be very different from the real one.

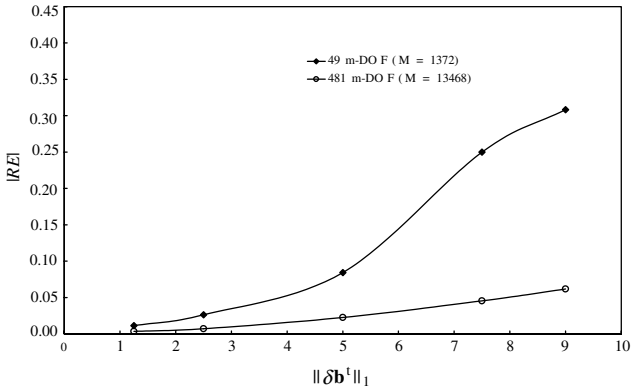

Fig. 7. Degree of damage and absolute value of RE with incomplete models (dynamic expansion).

3.2.2. With errors and without equations weighting or deletion

The presence of measurement noises and errors was simulated by incorporating a random perturbation of 5.0% error in the amplitudes of the m-DOF of the damaged structure. These errors were simulated by generating a random number $R \in [0, 1]$ in a uniform distribution. As in the previous sub-section, the equations relative to u-DOF are discarded.

The DME, FAE, MSE and RE values for the third damage case are presented in Table 7 and show that the presence of errors leads to incorrect damage identifications and have a strong influence on all the accuracy indicators. Note that the accuracy indicators with 481 m-DOF are equal and with 325 and 156 m-DOF are almost the same for dynamic and static expansions.

Table 6
Third damage case DME, FAE, MSE and RE values with incomplete models ($n = m = 40$, [50, 1900] Hz)

No. of m-DOF	No. of equations, M	Method	DME	FAE	MSE	RE
481	13468	Dynamic expansion	0.0000	0.0588	0.0090	−0.0226
		Static expansion	0.0000	0.0588	0.0090	−0.0226
325	9100	Dynamic expansion	0.0000	0.0588	0.0098	−0.0263
		Static expansion	0.0000	0.0588	0.0100	−0.0269
156	4368	Dynamic expansion	0.0000	0.0588	0.0080	−0.0255
		Static expansion	0.0000	0.0588	0.0083	−0.0260
49	1372	Dynamic expansion	0.1250	0.1250	0.0231	−0.0842
		Static expansion	0.2500	0.1429	0.0227	−0.0940

Table 7
Third damage case DME, FAE, MSE and RE values with incomplete models and 5.0% error in the amplitudes of the m-DOF ($n = m = 40$, [50, 1900] Hz)

No. of m-DOF	No. of equations, M	Method	DME	FAE	MSE	RE
481	13468	Dynamic expansion	0.0625	0.1667	0.0188	−0.0304
		Static expansion	0.0625	0.1667	0.0188	−0.0304
325	9100	Dynamic expansion	0.0625	0.2105	0.0158	−0.0713
		Static expansion	0.0625	0.2105	0.0158	−0.0720
156	4368	Dynamic expansion	0.0625	0.2105	0.0164	−0.0402
		Static expansion	0.0625	0.2105	0.0165	−0.0409
49	1372	Dynamic expansion	0.3125	0.1538	0.0321	−0.0898
		Static expansion	0.3750	0.0769	0.0334	−0.1017

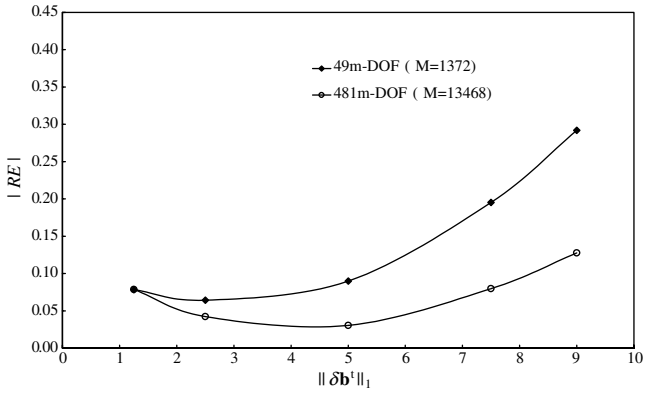

Fig. 8. Degree of damage and absolute value of RE with incomplete models and errors (dynamic expansion).

Fig. 8 shows a graphic that relates the degree of damage to the absolute value of RE when incompleteness and errors are both present. This graphic presents two distinct zones, for each case of incompleteness: (1) the continuous lines relate to the influence of errors alone. In fact, when the damage is small, the differences among the damage and undamaged structure behaviour will also be small and, therefore, the errors will overshadow this differences; (2) the broken lines indicate the influence of incompleteness, because the expansion of m-DOF is not sufficiently correct for large damage values (see Section 3.2.1). The first damage case presents almost the same value of RE for both 481 and 49 m-DOF. This seems to prove that the main influence is in fact the presence of errors.

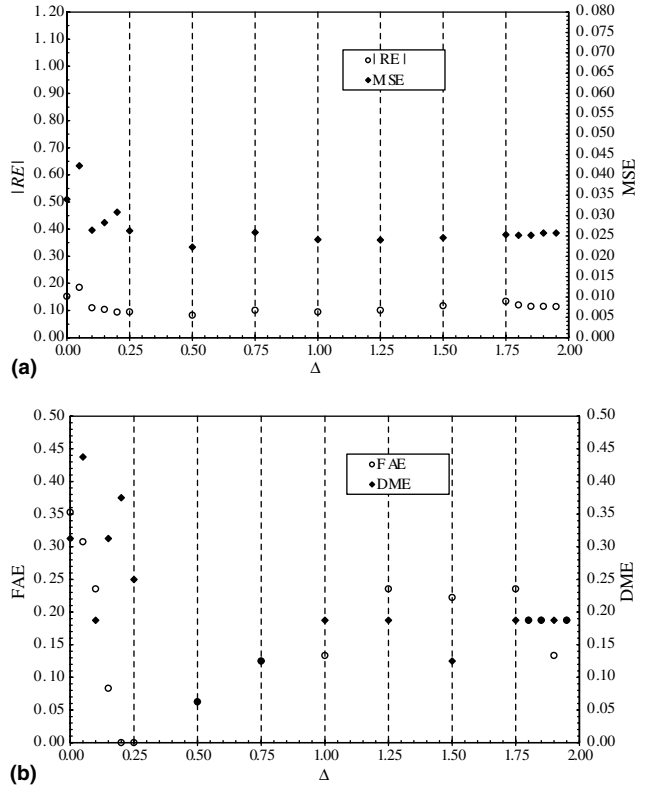

Fig. 9. Third damage case accuracy indicators in function of equations deletion parameter Δ (dynamic expansion of 49 m-DOF, 5.0% errors in the amplitudes of m-DOF): (a) |RE| and MSE, (b) FAE and DME.

3.2.3. With errors and equations weighting and deletion

In this sub-section is presented the study of the equations deletion parameter Δ, defined by Eq. (19). Fig. 9(a) presents the accuracy indicators |RE| and MSE in function of Δ for the third damage case, dynamic expansion of 49 m-DOF and 5.0% errors in the amplitudes of m-DOF. For $\Delta \in [0.50, 1.95]$ the values of these indicators are the lowest, with $|\mathrm{RE}| < 0.1400$ and $\mathrm{MSE} < 0.0260$. The minimum values of |RE| and MSE are obtained with $\Delta = 0.50$. However, not all the values of $\Delta \in [0.50, 1.95]$ present low values of FAE and DME (Fig. 9(b)). These two indicators show a minimum for

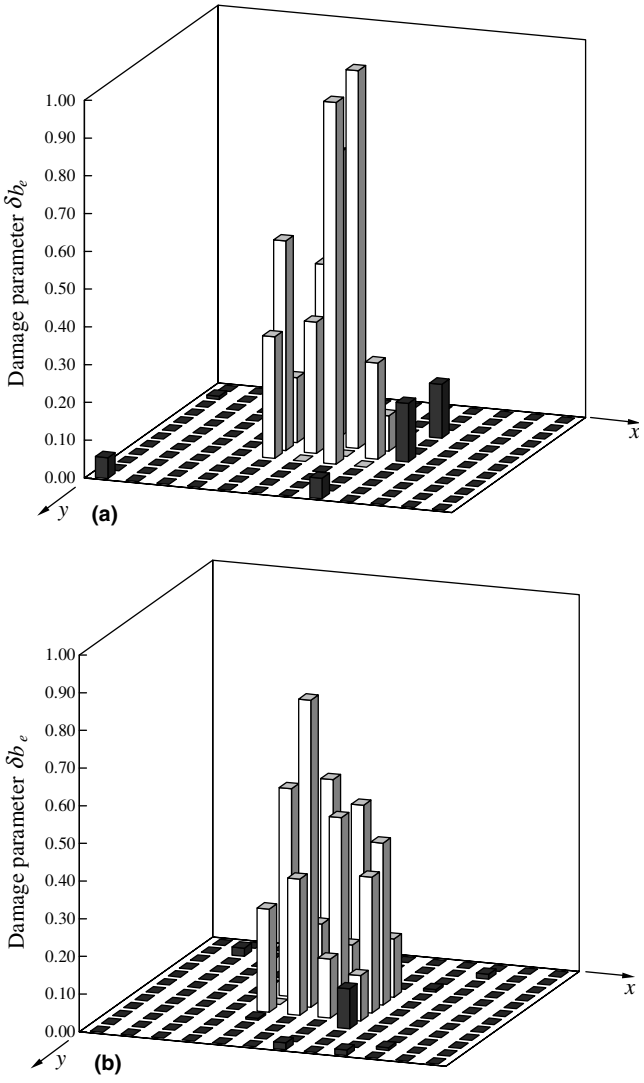

Fig. 10. Third damage case results (dynamic expansion of 49 m-DOF, 5.0% errors in the amplitudes of m-DOF): (a) no weighting and no deletion of equations ($M = 1372$), (b) weighting and deletion of equations with $\Delta = 0.5$ ($M = 423$).

$\Delta = 0.50$. Therefore, one can conclude that the best value of Δ is 0.50. Fig. 10 shows the identification results in all elements for the third damage case, dynamic expansion of 49 m-DOF and 5.0% errors in amplitudes of m-DOF. In Fig. 10(a) there are more false identified elements away from the real damaged area than in Fig. 10(b). Hence, the best results are in fact obtained by weighting and deleting equations.

3.3. FRF sensitivity technique versus modal sensitivity technique

Comparing the results presented in this paper with those in [12], it can be concluded that the FRF sensitivity technique results are better than those based on the modal sensitivity. One of the causes for this is that this last technique presents an underdetermined set of equations, whereas the technique presented here leads to an overdetermined set of equations.

4. Conclusions

In this paper a damage identification technique based on FRF sensitivities is presented. The set of linear equations obtained is solved using the bounded-variables least-squares algorithm, which constrains the solution to be physically admissible. The damage identification was performed on a laminated rectangular plate, discretised using a finite element model. It was found that the FRF matrices should be computed with at least three times the number of natural frequencies and mode shapes contained in the frequency range of interest. The frequency range and the excitation location are also important, and the better identification results are obtained in lower frequency ranges and excitation points were there are no nodes. The tests show that the dynamic expansion of m-DOF presents better results than those of the static expansion and as the number of m-DOF increases, there are an improvement in the results. It is demonstrated that for small damage the errors are the main influence in the identification quality, whereas for large damage the incompleteness becomes the most important factor. A procedure for weighting and deletion of equations is used to improve the identification results. It was also found that the present technique presents better results than those obtained when using a technique based on modal data sensitivities.

Acknowledgment

The authors would like to thank the financial support received from FCT and POCTI/FEDER (Projects POCTI/EME/12028/98/2001 and POCTI/2001/EME/37559).

References

[1] Doebling SW, Farrar CR, Prime MB, Shevitz DW. Damage identification and health monitoring of structural and mechanical systems from changes in their vibration characteristics: a literature review. LA-13070-MS. Los Alamos National Laboratory; 1996.
[2] Zou Y, Tong L, Steven GP. Vibration-based model-dependent damage (delamination) identification and health monitoring for composites structures—a review. J Sound Vib 2000;230(2):357–78.
[3] Stubbs N, Osegueda R. Global damage detection in solids-experimental verification. Int J Anal Exp Modal Anal 1990;5(2):81–97.
[4] Stubbs N, Osegueda R. Global non-destructive damage evaluation in solids. Int J Anal Exp Modal Anal 1990;5(2):67–79.
[5] Ricles JM, Kosmatka JB. Damage detection in elastic structures using vibratory residual forces and weighted sensitivity. AIAA J 1992;30(9):2310–6.
[6] Araújo dos Santos JV, Mota Soares CM, Mota Soares CA, Pina HLG. Identification of damage in composite structures: a numerical model. Mech Compos Mater Struct 1999;6(4):363–76.
[7] Araújo dos Santos JV, Mota Soares CM, Mota Soares CA, Pina HLG. Development of a numerical model for the damage identification on composite plate structures. Compos Struct 2000;48:59–65.
[8] Araújo dos Santos JV, Mota Soares CM, Mota Soares CA, Pina HLG. A damage identification numerical model based on the sensitivity of orthogonality conditions and least squares techniques. Comput Struct 2000;78(1–3):283–91.
[9] Kim J-T, Stubbs N. Improved damage identification method based on modal information. J Sound Vib 2002;252(2):223–38.
[10] Titurus B, Friswell MI, Starek L. Damage detection using generic elements: Part I. Model updating. Comput Struct 2003;81:2273–86.
[11] Titurus B, Friswell MI, Starek L. Damage detection using generic elements: Part II. Damage detection. Comput Struct 2003;81:2287–99.
[12] Araújo dos Santos JV, Mota Soares CM, Mota Soares CA, Maia NMM. Structural damage identification: Influence of model incompleteness and errors. Compos Struct 2003;62:303–13.
[13] Lin RM, Ewins DJ. Analytical model improvement using frequency response functions. Mech Syst Signal Process 1994;8(4):437–58.
[14] Wang Z, Lin RM, Lim MK. Structural damage detection using measured FRF data. Comput Methods Appl Mech Eng 1997;147:187–97.
[15] Modak SV, Kundra TK, Nakra BC. Prediction of dynamic characteristics using updated finite element models. J Sound Vib 2002;254(3):447–67.
[16] Kidder RL. Reduction of structural frequency equations. AIAA J 1973;11(6):892.
[17] Guyan RJ. Reduction of stiffness and mass matrices. AIAA J 1965;3(2):380.
[18] Mota Soares CM, Freitas MM, Araújo AL, Pedersen P. Identification of material properties of composite plate specimens. Compos Struct 1993;25:277–85.
[19] Maia NMM, Silva JMM, editors. Theoretical and experimental modal analysis. New York: John Wiley & Sons, Ltd; 1997.
[20] Ren Y, Beards CF. Identification of joint properties of a structure using FRF data. J Sound Vib 1995;186(4):567–87.
[21] Lawson CL, Hanson RJ. Solving least squares problems. Englewood Cliffs, NJ: Prentice-Hall, Inc; 1974.
[22] Stark PB, Parker RL. Bounded-variable least-squares: an algorithm and applications. Comput Statist 1995;10:129–41.
[23] Kim J-T, Stubbs N. Model-uncertainty impact and damage-detection accuracy in plate girder. J Struct Eng 1995;121(10):1409–17.

[24] Yun C-B, Yi J-H, Bahng EY. Joint damage assessment of framed structures using a neural networks technique. Eng Struct 2001;23:425–35.
[25] Zienkiewicz OC. The finite element method in engineering science. New York: McGraw-Hill; 1971.
[26] Bathe K-J. Finite element procedures. Englewood Cliffs, New Jersey: Prentice-Hall; 1996.
[27] Friswell MI, Mottershead JE. In: Finite element model updating in structural dynamics. Solid Mechanics and its Applications, vol. 9. The Netherlands: Kluwer Academic Publishers; 1995.
[28] Grafe H. Model updating of large structural dynamics models using measured response functions. PhD thesis. Imperial College of Science, Technology and Medicine, University of London; 1999.